Chemometrics and Intelligent Laboratory Systems 226 (2022) 104588

Contents lists available at ScienceDirect

Chemometrics and Intelligent Laboratory Systems

journal homepage: www.elsevier.com/locate/chemometrics

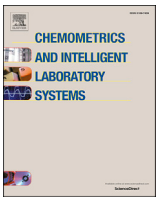

Sequential multiblock partial least squares discriminant analysis for assessing prostate cancer aggressiveness with multiparametric magnetic resonance imaging

E. Aguado-Sarrió [a,b,*], J.M. Prats-Montalbán [a,b], R. Sanz-Requena [c,d], C. Duchesne [e], A. Ferrer [a,b]

[a] Kenko Imalytics S.L., Avda. Médico Vicente Torrent 8, 46015, Valencia, Spain
[b] Grupo de Ingeniería Estadística Multivariante (GIEM), Universitat Politècnica de València (UPV), Valencia, Spain
[c] Área de Radiología Cuantitativa y Biomarcadores de Imagen, Servicio de Radiología, Hospital Quironsalud Valencia, Valencia, Spain
[d] ICT Department, Florida Universitària, C/ Rei en Jaume I, 2, 46470, Catarroja, (Valencia), Spain
[e] Department of Chemical Engineering, Université Laval, G1V 0A6, Québec, QC, Canada

A B S T R A C T

In current radiology practice, multi-parametric magnetic resonance imaging (mpMRI) has recently become a key tool in diagnostic and therapeutic decisions. Although it is based on the subjective assessment of T2-weighted images, as well as perfusion-weighted and diffusion-weighted sequences, further quantitative parameters can also be derived from them for improving lesion phenotyping. Despite these parameters are usually exploited in a univariate way, ignoring the benefits of a real multivariate approach, still it is the gold standard imaging technique to assess prostate cancer location and probability of malignancy. In this paper, pharmacokinetic (perfusion) and exponential (diffusion) clinical models, as well as latent variable-based multivariate statistical models like multivariate curve resolution-alternating least squares (MCR-ALS), have been calculated and analyzed with sequential multi block-partial least squares discriminant analysis (SMB-PLS-DA) including technique-block differentiation, in order to better assess for cancer aggressiveness based on Gleason scales. The best prediction result was achieved by the ordered combination of diffusion blocks (MCR-ALS and exponential models) and normalized T2 values. The perfusion blocks did not improve the results obtained by diffusion and T2-weighted based parameters alone, so they can be removed from the SMB-PLS-DA model.

1. Introduction

Currently, medical imaging is a key information source for tumor detection, grading and staging. Classical MR sequences, such as T1-weighted (T1w) or T2-weighted (T2w), provide excellent spatial and temporal resolutions using non-ionizing radiations, in a minimally invasive way. They have been used to evaluate normal structures and tumor morphological features [1]. The development of functional sequences has allowed estimating and understanding the complex physiological characteristics of tumors in a non-invasive way, providing knowledge on tumor vascularization and cellularization; thus improving detection, tracking and tracing of these malignant tumor processes. Vascularization is divided into two phenomena: a) the creation of new vessels (angiogenesis) or b) the development of existing ones (neovascularization); when a group of growing cells presents abnormally high demands of oxygen and nutrients. Cellularization, on the other hand, is related to cell proliferation and agglomeration in some local tissue region. Since the combination of these phenomena is related to early tumor aggressive oncogenesis, functional MR imaging provides complementary information to that obtained from conventional imaging.

There are two main functional MR imaging sequences: dynamic contrast-enhanced MR (DCE-MR) imaging for perfusion assessment [2] and diffusion-weighted MR (DW-MR) imaging for water diffusibility assessment [3,4]. The combination of T2w with these imaging sequences is commonly known as multiparametric MR (mpMR).

In perfusion (DCE-MR) studies, an exogenous gadolinium (Gd) based contrast media is administered intravenously, going from the capillary network into the extravascular extracellular space (EES), afterwards returning to the vascular system and being progressively filtered by the kidneys. This process establishes a dynamic relationship between the image signal intensity changes and the amount of contrast media that passes into the tissues. Fitting these intensity-versus-time curves to specific parametric models allows obtaining quantitative dynamic measurements.

In diffusion (DW-MR) studies, the signal intensity is related to the

* Corresponding author. Kenko Imalytics S.L., Avda. Médico Vicente Torrent 8, 46015, Valencia, Spain.
E-mail address: eric@kenkoimalytics.es (E. Aguado-Sarrió).

https://doi.org/10.1016/j.chemolab.2022.104588
Received 18 February 2022; Received in revised form 8 May 2022; Accepted 17 May 2022
Available online 25 May 2022

movement of protons and T2w by measuring the loss of coherence or synchrony between the water protons; being progressively reduced according to a factor (b-value [5]). This attenuation depends on the characteristics of the tissue, being stronger if the tissue is highly vascularized, and reduced if highly cellularized. The range of different signal attenuations between tissues at the same b-value is the basics to extract biological information from different behaviors in the diffusion processes.

Despite these quantitative measurements from complex MR equipments, the assessment of prostate mpMR images is usually performed qualitatively, following the so-called Prostate Imaging Reporting and Data System (PI-RADS) guide [6]. PI-RADS allows detecting and characterizing prostate lesions, by assigning some probability of malignancy based on specific image findings. However, this methodology is subjective and suffers of certain discrepancies, as it is not based on quantitative data. Moreover, lesion aggressiveness cannot be properly assessed. One alternative to overcome this problem is to compute quantitative parameters from functional MR imaging. These parameters will be considered imaging biomarkers if they are objectively measured (give quantitative information) and behave as an indicator of a normal biological process, a disease, or a response to therapy [7].

Imaging biomarkers can be used for determining biological properties related to the tumor growth or aggressiveness. To do so, it is mandatory to fit and characterize the intensity versus time (in the case of DCE-MR) or versus b-value (in the case of DW-MR) curves associated to each pixel of the images. Although pharmacokinetic models [8] (in the case of DCE-MR) and exponential models [9,10] (in the case of DW-MR) have the ability to provide clinically-oriented biomarkers in tumor analysis, their interpretation is not easy nor direct in many cases; so new biomarkers obtained from latent variables-based multivariate statistical models, like multivariate curve resolution (MCR [11–13]), have recently been also proposed [14–17] to improve prostate cancer assessment.

This paper deals with a high relevant problem in MR imaging: selecting the best type of MR sequence (diffusion, DW-MRI; or perfusion, DCE-MRI), afterwards selecting the best biomarkers (MCR-based or clinical models-based). Within each type of sequence. All this with the final goal of classifying the aggressiveness of a tumor (prostate cancer in this case). These sequences are complex data structures, with 2D images gathered at different time points (DCE) or b-values (magnitude of the applied magnetic field; DW), at different slices of the organ under study (prostate in this case). Therefore, it is convenient to summarize these sequences in a reduced number of new images with physiological meaning, i.e. imaging biomarkers. Since these physiological behaviors are not orthogonal, we propose to apply MCR to unravel these "hidden dynamics".

However, not only MCR-based imaging biomarkers, but also those calculated from clinical models (the commented pharmacokinetic and exponential models), are available, making the selection of the best set not only a difficult task, but actually unaffordable in many practical cases, due to the lack of complete knowledge, or simply because of clinical routine. So, it is relevant to compare them and see their benefits is terms of classification.

In order to deal with different and multiple sources of information, multiblock methods are applied. These techniques were preferred against Partial Least Squares (PLS) [18,19] due to their ability to separate the information block-by-block instead of selecting individual variables (biomarkers), no matter which type of image sequence (DCE or DW) or biomarker calculation technique (clinical or latent variable models) they come from. This is important from a practical point of view because it allows to entirely eliminate blocks of unnecessary information associated to the type of image sequence or the biomarker calculation model, and select only the most useful blocks to characterize the aggressiveness of the prostate tumor. This may make it possible that only one type of MR imaging sequence (DCE or DW) needs to be performed (with a consequent reduction in the time that the patient is undergoing radiological tests) and that only one method (clinical or latent variable-based) needs to be used for the calculation of biomarkers (reducing computation times and, therefore, speeding the delivery of radiological reports).

In this paper, sequential multiblock PLS model [20–22] in its discriminant version (SMB-PLS-DA), was proposed to compare different groups of imaging biomarkers. This sequential multiblock model was preferred to other multiblock approximations because of its ability to extract orthogonal information for each block in a consecutive way (block-after-block), grouping the correlated information or discarding the unnecessary latent variables. Thus, it was possible to detect those truly relevant blocks in the tumor aggressiveness differentiation and, after that, the ones that do not supply additional discriminating power with respect to the previous blocks were removed.

The paper is organized as follows. In Section two the database of patients and the different clinical and latent variables-based multivariate statistical models are presented. Then, the proposed iterative method for classification performed with SMB-PLS-DA is detailed. Section three presents the results of the statistical comparison and discusses the pros and cons of combining different types of MR sequences. Finally, Section four shows the conclusions.

2. Materials and methods

2.1. Patient database

DCE-MR and DW-MR sequences from 36 histologically-confirmed cases of peripheral prostate tumors were acquired, ensuring full prostate coverage (16 slices, in-plane resolution of 192 × 192 voxels, each one measuring 1.56 × 1.56 × 4 mm^3). DCE-MR and DW-MR sequences were acquired at 47 time points (overall acquisition time 5 min) or 6 different b-values (0, 50, 200, 400, 1000, 2000 s/mm^2), respectively. The high resolution T2w images were acquired covering the full prostate with 25 slices, an in-plane resolution 512 × 512 voxels, and a 0.49 × 0.49 × 3 mm^3 voxel size. An example of a DCE-MR sequence is shown in Fig. 1:

Reference tumor regions of interest (ROIs) were manually segmented for the peripheral zone of the prostate, considering image findings (PI-RADS criteria) and spatial correlation with biopsy location. To study aggressiveness, only the ROIs associated to dominant lesion (DL) were considered. The pathologic Gleason score was selected as a regularized indicator of the level of malignancy [23], being used to separate the lesions into two categories for classification: low aggressiveness (LA) when Gleason $\leq$6 and high aggressiveness (HA) when Gleason $\geq$7. The final database was composed of 36 biopsied areas in a balanced way (18 LA and 18 HA) from different patients.

All patients gave consent for using their medical images, which were anonymized before post-processing. The local Ethics Committee approved the study protocol.

2.2. Clinical models

2.2.1. Perfusion pharmacokinetic modeling

In radiology, pharmacokinetic (PHK) models try to characterize the absorption, distribution and excretion dynamics of an injected contrast agent within a tissue. Compartmental models have been proposed to describe these tissue dynamics, considering the intravascular and the extracellular extravascular (EES) spaces as main compartments. Three different models were considered, clustered into two groups according to complexity. On one hand, the so-called "classical" or "first-generation" models: the Tofts model (or its extended version, i.e., Tofts extended model) and on the other hand the models belonging to the so-called

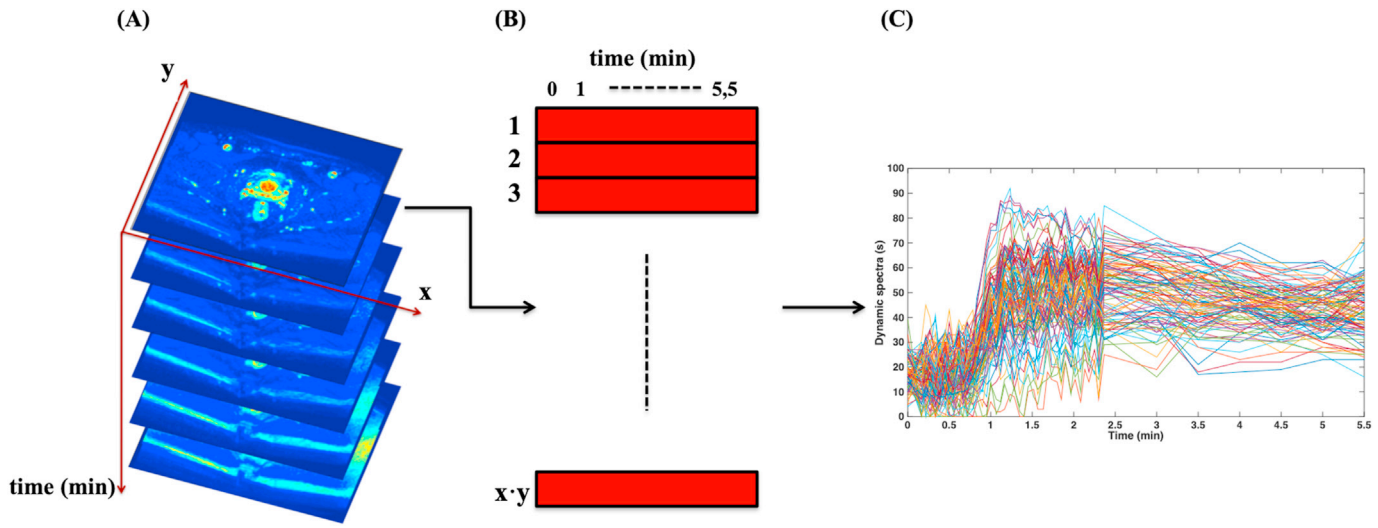

Fig. 1. (A): 3D data structure for a specific slice of one case of DCE-MRI; x and y are the spatial resolution of the image, t is the number of time points for perfusion. (B): Unfolded 2D matrix. (C): Dynamic spectra evolution along time, showing signal intensity for a specific slice of the prostate.

"second-generation" models: the 2-compartment exchange model (2CXM) and the adiabatic approximation to tissue homogeneity (AATH) model [8]. A detailed formulation explanation can be found in Refs. [17,24]. In these models, the vascular and EES volumes can be represented as a system of partial differential equations where the contrast is exchanged between different subspaces. They can be solved analytically by expressing the contrast concentration $C(t)$ as a convolution product of the concentration of the arterial input function ($C_{AIF}(t)$) and the $R(t)$ function, which is the analytical solution of these systems. The contrast concentration $C(t)$ is directly related with the DCE-MR signal intensity of each pixel at each time point $I(t)$. In this paper, $C(t)$ was obtained from $I(t)$ using a direct conversion based on contrast media relaxivity and field strength.

$$C(t) = (C_{AIF} * R)(t) \tag{1}$$

In this expression, $R(t)$ only depends on the first (K^{trans}, k_{ep}, v_e) or second (Fp, PS, v_e, v_p) generation perfusion biomarkers [8,24] at each time instant t. In order to obtain these biomarkers, the models need as input the reference arterial input function ($C_{AIF}(t)$), which was calculated in this paper using a principal component analysis (PCA) model [25], by automatically selecting the pixels related to a pure arterial dynamic pattern [26]. Once the $C_{AIF}(t)$ was individually calculated for each patient, the perfusion sequence was analyzed pixel-by-pixel and the biomarkers were calculated using non-linear optimization algorithms. It must be strengthened, however, that these pharmacokinetic models assume some a priori knowledge about the dynamics followed by tissues. As tumoral lesions produce new vessels and stroma in a chaotic way, the dynamics might not behave as expected. It seems then necessary to establish some parameters in order to evaluate the goodness of fit of the dynamic behaviors, to evaluate the reliability of the obtained biomarkers. However, in clinical practice, the values of the biomarkers are usually obtained without any information about such a fit and applied directly for tumor diagnosis and/or prognosis. In order to tackle this issue, this paper introduces the use, not only of these biomarkers, but also of the Residual Sum of Squares (*RSS*) as a complementary biomarker (parameter) providing information about how well the pixel was fitted by the assumed model, measuring the disagreement between each pixel behavior, and its prediction from the assumed model. By computing and storing the *RSS*, the model not only provides the value of the biomarker but also its reliability.

2.2.2. Diffusion exponential modeling

The signal decay of the DW-MR sequences is a function of the diffusion b-value and can be fitted with different approaches. The most widely used is the monoexponential model [9], whose apparent diffusion coefficient (*ADC*) associated parameter integrates the global effect of the slow displacements (intracellular and interstitial) as well as fast movements due to intravascular diffusion. The main problem is that the monoexponential model does not consider the different mechanisms of the diffusion process. Currently, one way of dealing with this problem is by using a two-exponential model known as intra-voxel incoherent motion (IVIM) [10]. This more complex model considers two behaviors, slow and fast diffusion, weighted by a parameter called vascular fraction (f), which relates to the proportion of vascular tissue in a pixel. This model is able to separate these two effects from the pixel signal decay with increasing b-values [27,28]. This way, it is possible to quantify and segregate the slow diffusion (real diffusion) due to extravascular spread (cellularization), from fast diffusion (pseudo-perfusion) due to vascularization [29].

Despite the fact that the IVIM model is theoretically more appropriate according to physiological criteria, the monoexponential model is the most widely used due to its simplicity. A detailed explanation of the model definition and calculation can be found in Ref. [15]. Additionally, the *RSS* was also calculated as an additional biomarker for the same reasons (i.e. assessing biomarkers reliability) explained in the perfusion section.

2.3. MCR-ALS models

One characteristic of clinical models is the lack of a priori knowledge about the tissue patterns, which leads to a series of assumptions conditioning the use of different approaches [28]. Accordingly, and depending on tissue patterns, the clinical models may provide biased measurements, which may not properly reflect the true physiology of the tissue [10,30]. Therefore, a priori knowledge about the tissue behaviors might help interpreting the information provided by the imaging biomarkers.

One possible way to look for physiological meaningful dynamics is by applying latent variable-based multivariate statistical models to the DCE/DW-MR data. Multivariate Image Analysis deals with the application of

multivariate statistical projection models, commonly on gray-scale, color, multi and hyper spectral images, but also on MRI or quite recently ultrasound images [31,32], usually based on PCA [25]. Its application to oncology [33] allows extracting the sources of variation from a relevant number of time-sequenced images from different individuals, providing new latent variable-based statistical models that help explaining the differences between healthy and tumor tissues.

Nevertheless, a relevant drawback of the application of PCA in DCE-MR image analysis is that the estimated dynamics patterns are forced to be orthogonal. The orthogonality of the principal components is a limitation to model different perfusion behaviors that are not necessarily orthogonal. In order to overcome these drawbacks, it is possible to use more flexible models, which do not impose this restriction, like Multivariate Curve Resolution-Alternating Least Squares (MCR-ALS) [11–13]. MCR is preferred to PCA because of its ability to provide physiologically more interpretable behaviors by imposing a priori knowledge on the model. MCR-ALS is an iterative method that performs a bilinear decomposition of an **S** matrix containing the signal intensity registered for each pixel in rows by means of an alternating least squares optimization algorithm.

$$\mathbf{S} = \mathbf{C}(\mathbf{D})^{\mathrm{T}} + \mathbf{E} \tag{2}$$

$\mathbf{D}^{\mathbf{T}}$ is a matrix containing in its rows each of the pure behaviors (pure spectrum associated to each physiological phenomena); **C** gathers in its rows the relative contribution of each behavior for each pixel of the image; and **E** is a residual matrix [14–16,24].

By refolding the **C** matrix into the original spatial dimensions, new parametric images can be obtained, which allows locating those pixels more related to each one of the corresponding modeled behaviors. In this case, equal length normalization was applied to $\mathbf{D}^{\mathrm{T}}$ matrix during the MCR-ALS iterative process in order to obtain concentrations (**C**) that can be directly compared between them.

The process of obtaining the number of components and the initial estimation of $\mathbf{D}^{\mathrm{T}}$ matrix was described in previous works [14–17]. Briefly, two components (referred to true behaviors) were considered for the MCR models, using the concentrations as their corresponding biomarkers: in perfusion, normal tissue (*NT*) and highly vascular tissue (*VT*) types); and in diffusion, fast (d_1) and slow (d_2) exponential decays. An illustrative example is shown in Fig. 2.

Additionally, the residual sum of squares (*RSS*) of the MCR models was included as a potential biomarker measuring the disagreement between each pixel behavior and its prediction from the assumed model.

MCR-ALS is based on an iterative process that can provide infinite solutions for the same data matrix, causing a problem known as ambiguity in the solution. This problem can be relieved by imposing constraints based on prior knowledge [34], so that it is possible to obtain easier-to-interpret solutions. In this paper, two additional constraints were imposed:

- Non-negativity on the pixel concentration **C** values, because the intensity in a pixel has to be nonnegative. Also, non-negativity on the behavior profiles $\mathbf{D}^{\mathrm{T}}$.
- Exponential shape of the pure behaviors $\mathbf{D}^{\mathrm{T}}$ (only in diffusion).

The ambiguity in the solution problem has been checked in previous works through MCR-bands [35], where the tuned bands were very close to the proposed solution and the pure behaviors found can be considered unambiguous.

One problem arises when combining imaging biomarkers obtained from different MR sequences, taken at different time or positioning, known as the "alignment problem". When using different types of sequences, it is not possible to ensure that the location of each pixel of e.g., the diffusion sequence corresponds exactly to the same pixel in the perfusion sequence (it might happen due to small movements and change of image resolution). In order to solve this alignment problem, it is mandatory to apply image registration methods. In medical image (among other areas), registration methods are those that modify the spatial resolution and correct the position of one sequence with the aim of aligning it to another sequence (reference sequence), i.e. making every pixel from the secondary sequences to exactly correspond to the same pixel of the reference sequence. In this paper a simple registration

Table 1
Data block structure. The number of variables is obtained after multiplying the descriptive statistics (mean, median, variance, P25, P75, skewness, kurtosis), by the number of biomarkers provided by each perfusion or diffusion model and T2w.

Blocks	Models	Imaging biomarkers	# variables
(1) Exp. Model-based DWI	Monoexponential, IVIM	*ADC*, *D*, *D**, *f*, *RSS* (x2)	42 (6 × 7)
(2) MCR-DWI	MCR-ALS (Diffusion)	d_1, d_2, *RSS*	21 (3 × 7)
(3) PHK model-based DCE	Extended Tofts, AATH, 2CXM	K^{trans}, k_{ep}, v_e (x3), v_p (x3), *Fp* (x2), *PS* (x2), *RSS* (x3)	105 (15 × 7)
(4) MCR-DCE	MCR-ALS (Perfusion)	*NT*, *VT*, *RSS*	21 (3 × 7)
(5) Normalized T2w	–	Muscle-normalized *T2w* [a]	7

[a] muscle-normalized T2w was calculated dividing the intensity of the image by the intensity of the muscle.

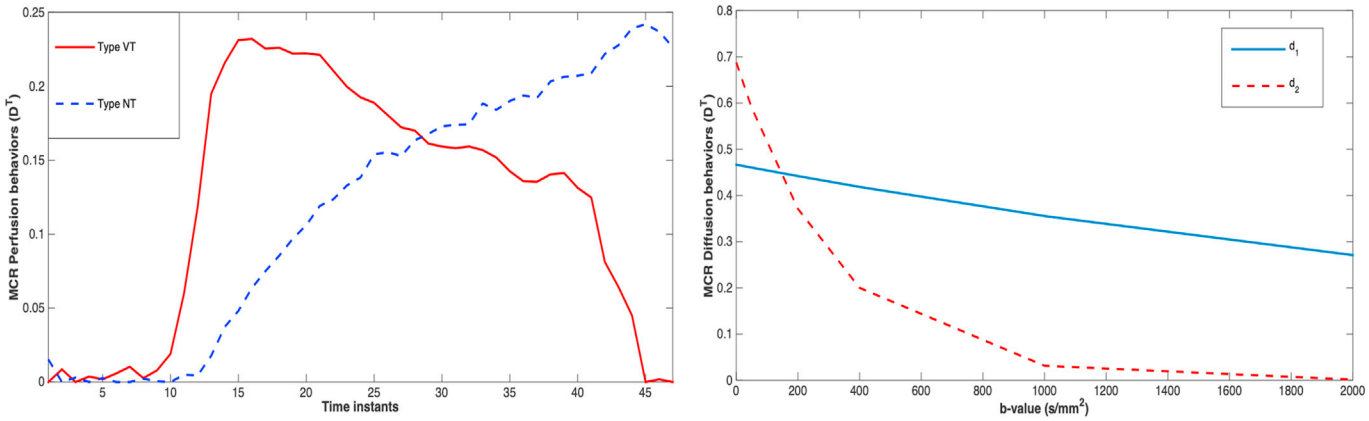

Fig. 2. Illustrative example: (Left) Behaviors obtained from MCR-ALS perfusion model, representing *VT* (vascularized tissue, solid) and *NT* (normal tissue, dotted). (Right) Behaviors obtained from MCR-ALS diffusion model, representing d_1 (slow diffusion, solid) and d_2 (fast diffusion, dotted).

method based on a linear transformation taking into consideration some reference points was used with satisfactory results. In this method, the specialists manually select two reference points for each spatial direction (x, y and z) corresponding to the limits of the organ. These points are needed for both sequences (reference and secondary) and should be taken individually for each patient. It consists on determining the position where each pixel of the secondary sequences from the original sequence (the one taken during the acquisition) needs to be moved, considering their position in the reference sequence. For more insight, the reader is referred to Ref. [17].

2.4. SMB-PLS-DA and iterative procedure method

2.4.1. SMB-PLS-DA

Imaging biomarkers were obtained for all the pixels of the ROIs described in section 2.1. In order to characterize a dominant lesion composed by several pixels, different statistical descriptors from each imaging biomarker were calculated for each ROI: mean, median, standard deviation, 25% percentile (P25), 75% percentile (P75), skewness and kurtosis. The data block structure is summarized in Table 1.

The input matrix **X** is arranged in 5 blocks of variables ($B = 5$ [$\mathbf{X}_1$ … $\mathbf{X}_5$]) according to Table 1, where the rows are assigned to the ROIs. Matrix **Y** is defined with two columns of dummy variables for the same ROIs. The first column defined the "LA" variable: value 1 if the ROI is a lesion with low aggressiveness (i.e. Gleason≤6), and 0 if it shows high aggressiveness (i.e. Gleason≥7). The second column is the "HA" variable and is built complementary to the first one. Then, SMB-PLS-DA is applied.

The steps of the procedure follow:

1. Obtain the MCR and clinical biomarkers from the magnetic resonance sequences
2. Compute the different statistical descriptors from each imaging biomarker for each ROI.
3. Build the **X** matrix blocks joining the corresponding biomarkers statistics in one data array (blocks 1 to 5, see Table 1 for further details).
4. Build the **Y** matrix with two columns of dummy variables for the same ROIs. "LA" and "HA".
5. Apply SMB-PLS-DA.

SMB-PLS-DA uses the MB-PLS hierarchical structure where the variables are organized in different groups or "blocks" associated with different sources of information known as "regressor blocks" ($\mathbf{X}_b$). But, in this case, SMB-PLS-DA imposes a sequential pathway in order to sequentially extract information from each of them. A brief explanation of the SMB algorithm is described as follow:

The first step of the algorithm is to compute the block weights ($\mathbf{w}^T_1$) by the regression of an initial **Y** score **u** onto $\mathbf{X}_1$, followed by the calculation of the scores ($\mathbf{t}_1$) from the first block. Then, in order to differentiate the correlated information from the orthogonal information, the subsequent blocks ($\mathbf{X}_b$) ($b > 1$) were split using the following equation:

For $b = 1,2 \ldots B\text{-}1$ and $k = 1,2 \ldots B\text{-}b$

$$\mathbf{X}^{corr}_{b+k} = \mathbf{t}_b \cdot \left(\mathbf{t}^T_b \cdot \mathbf{t}_b\right)^{-1} \cdot \mathbf{t}^T_b \cdot \mathbf{X}_{b+k} \quad (3)$$

These blocks contain the correlated information with $\mathbf{X}_1$. After this, the block score for the subsequent block are computed by regressing **u** onto $\mathbf{X}^{corr}_b$ to obtain the block weights $\mathbf{w}^{T,corr}_b$. Next, the block score [$\mathbf{t}_1$ … $\mathbf{t}_b$] are combined in the super level score **T**. The last step is the computation of a PLS cycle between **u** and **T** to compute the super level weights ($\mathbf{w}_T$) and the super scores $\mathbf{t}_T$. This computation cycle is repeated until convergence on $\mathbf{t}_T$. Deflation of all $\mathbf{X}_b$ using the super scores is then performed. The procedure is repeated for computing the next component using the residuals of all data blocks. It continues to extract components from the first **X**-deflated block in the sequence until it has modeled all relevant information from **Y**. Any criteria available for selecting the number of components in latent variable methods can be used.

Once all the information from $\mathbf{X}_1$ has been explained, the same methodology is applied to the subsequent blocks. Since only the correlated information with the previous block was removed by the deflation step, the components for the subsequent block will only model new information not explained by the previous components. For the last block in the sequence, a regular PLS model is fitted to the $\mathbf{X}_B$ and **Y** residuals. The pseudo-code of the SMB-PLS algorithm [22] can be found in Annex 1.

2.4.2. Iterative procedure method

The proposed iterative method takes the basic idea of the SMB-PLS [20–22] model of extracting only the relevant latent variables from each block. In this paper, it was extended to the discriminant analysis

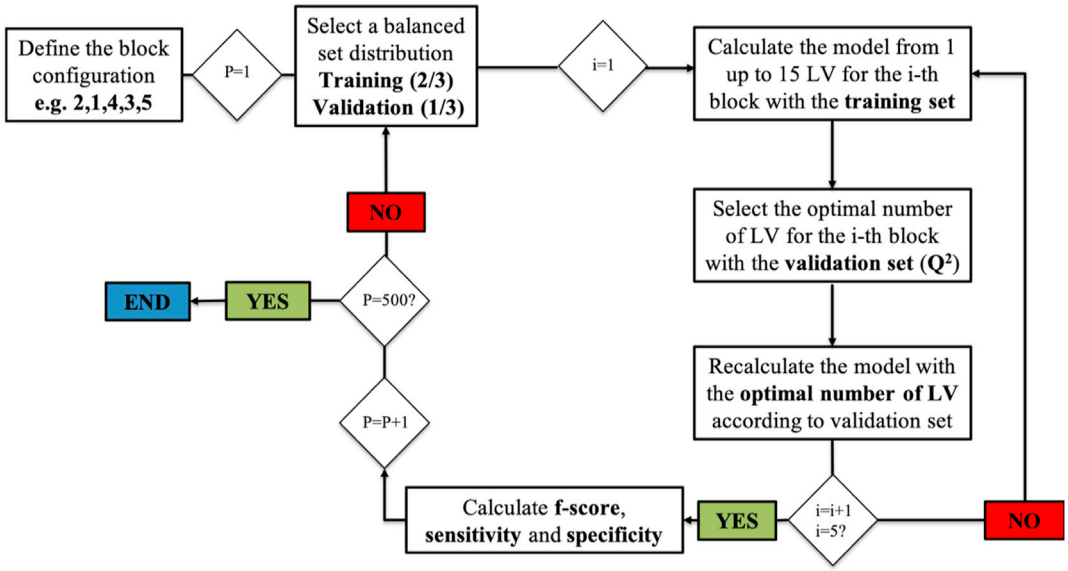

Fig. 3. SMB-PLS iterative process scheme for each blocks configuration, repeated 500 times to obtain the results for each proposed model. *P* represents the number of the iteration and *i* corresponds to the block in the *i*-th position (1–5) in the configuration. LV is referred to the number of latent variables. The block identifier is defined in Table 1.

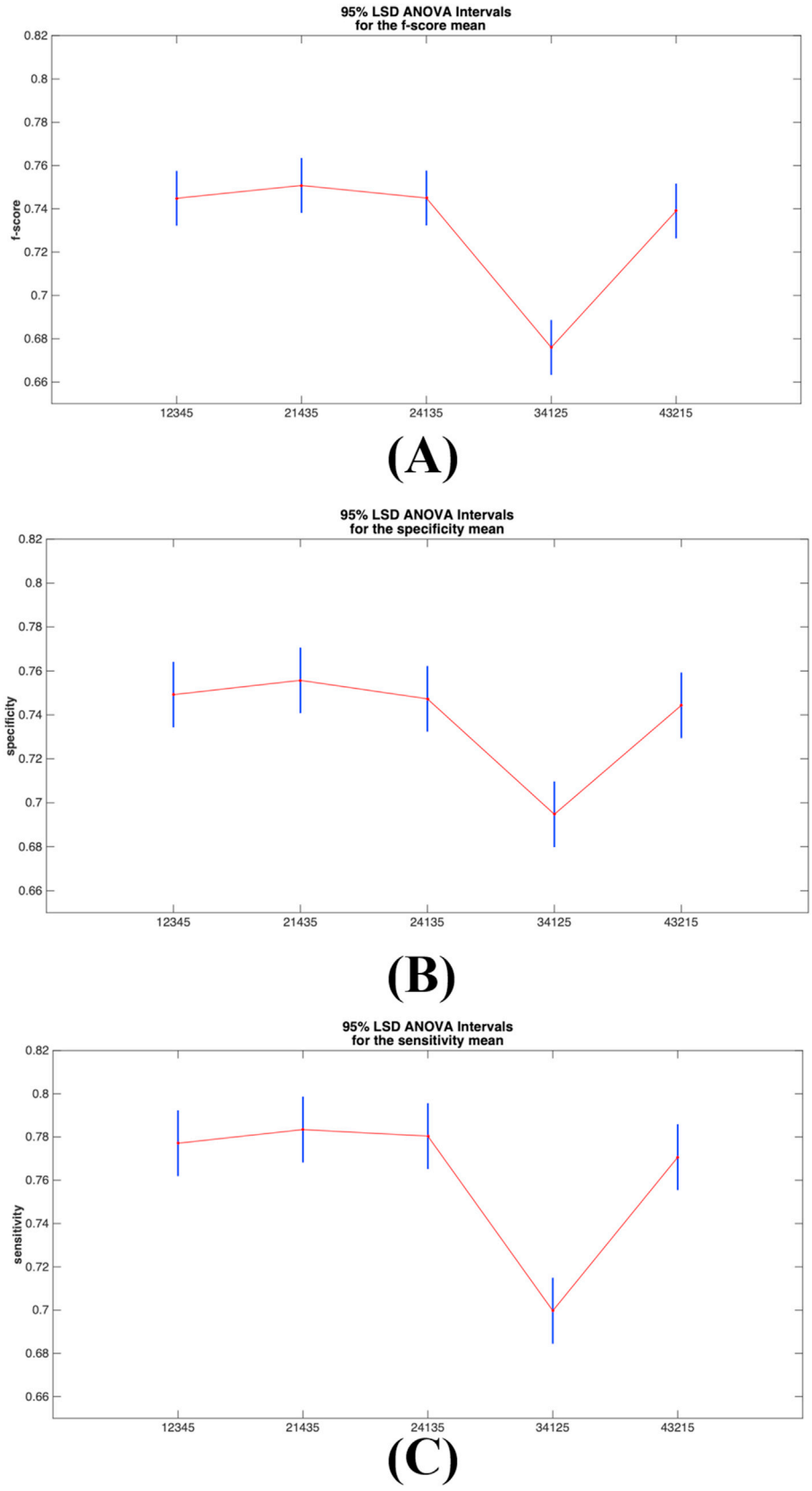

Fig. 4. 95% ANOVA LSD intervals for the average f-score (A), specificity (B), and sensitivity (C), of the different block configurations. The code for the configurations is defined in Table 1.

version of PLS with the objective of classifying the ROIs in two different categories (LA and HA).

The method consists in selecting two different balanced sets in a proportion 2/3 (24 ROIs) for training and 1/3 (12 ROIs) for validation for each iteration. First, it was necessary to establish the block ordering prior to applying SMB-PLS (this sequential order remained constant during the iterative loop represented in Fig. 3). Although from a clinical point of view, it is generally assumed that diffusion is preferred over perfusion as the best technique for assessing tumor aggressiveness, in this paper we evaluated different ordering between perfusion and diffusion blocks in order to check this assumption. The only special consideration is that T2w was always sequenced in the latter position as it is usually used as a complementary morphological image for improving clinical interpretation and diagnosis.

To start the algorithm, the block input sequence order has to be manually determined. Then, the SMB-PLS-DA model was calculated for the training set using simple cross-validation (CV) and a fixed number of latent variables (this paper has considered 15 as the maximum possible number of latent variables for each block because after many simulations, the optimal number of components never surpassed this value). Then, the projection of the validation set on this model was calculated, obtaining the goodness of prediction parameter Q^2 for the **Y** matrix at each number of latent variables. The number of optimal latent variables was that maximizing the Q^2 (validation) of the projection of the validation set on the model. Hereafter, the model was recalculated with the selected number of latent variables for that specific block using the training set and the validation set together, and then, the same procedure was applied for the next block until all the blocks were included (or not) in the model with their respective number of optimal latent variables. It should be noted here that a double cross-validation procedure, with a training, validation and (external) test set, would have been preferred, but it was not convenient to apply because of the small sample size. However, this is not so relevant when the final goal is not to assess some figure-of-merit performance (e.g. f-score), but to compare between approaches, since all of them are affected by the procedure in the same way.

Once the optimal model was obtained, the values of the final f-score, selectivity, specificity, the percentage of true negatives (TN), true positives (TP), false positives (FN), false negatives (FP) and the selected LV for each block of the optimal model obtained for each distribution of the groups (iteration) were stored. Therefore, the different values for the figures-of-merit (f-score, sensitivity and specificity) were calculated as follow:

$$\text{fscore} = \frac{2 \cdot \text{precision} \cdot \text{recall}}{\text{precision} + \text{recall}} \tag{4}$$

$$\text{precision} = \frac{TP}{TP+FP} \text{recall} \quad \text{or} \quad \text{sensitivity} = \frac{TP}{TP+FN} \text{specificity} = \frac{TN}{TN+FP} \tag{5}$$

Finally, the process was repeated again with the next configurations, obtaining, at the end, another improved model for each iteration (500 iterations per each proposed configuration). A scheme of the algorithm is shown in Fig. 3.

3. Results and discussion

The results are presented in two steps according to two different studies:

1. Analyzing the importance of the block order.
2. Analyzing the importance of block inclusion.

In the first step, five different configurations were considered:

- Prioritizing diffusion over perfusion, and clinical models (Pharmacokinetics and exponential) over MCR-ALS (12345).
- Prioritizing diffusion over perfusion, and MCR-ALS over clinical models (21435).
- Prioritizing MCR-ALS over clinical models, and diffusion over perfusion (24135)
- Prioritizing perfusion over diffusion, and clinical models over MCR-ALS (34125).
- Prioritizing perfusion over diffusion, and MCR-ALS over clinical models (43215).

Note that the T2w block (5) is always sequenced last because, as already commented, it always acts in clinical practice as a complementary morphological image. Anyway, we already ran new simulations placing the T2w block in the first position but it did not affect the results in the f-score classification index (results not shown).

In a second step, the iterative process was repeated but, in this case, some of the blocks were removed in order to study if the inclusion of the block matters. The aim was two-fold: to replicate the same results with a more parsimonious model; and to study the relevance of each MRI technique in terms of performance to assess tumor aggressiveness. This time, six different configurations were proposed:

- Removing the perfusion blocks (125).
- Removing the diffusion blocks (345).
- Removing perfusion + T2w (12).
- Removing diffusion + T2w (34).
- Removing perfusion + MCR DWI models (15)
- Removing perfusion + clinical (Exp. model-based) DWI (25)

The configurations 125 and 345 were proposed in order to study the absence of the imaging techniques: perfusion and diffusion, respectively. Then, configurations 12 and 34 were proposed in order to check the importance of T2w.

Table 2
Results summary for each proposed configuration. The number of optimal LV were calculated as the average values. The code for the configurations is defined in Table 1.

Conf.	Average # LV in block 1	Average # LV in block 2	Average # LV in block 3	Average # LV in block 4	Average # LV in block 5
12345	3.78	4.16	3.02	2.93	1.48
21435	3.69	5.00	2.24	4.27	1.56
24135	3.84	4.87	2.11	3.28	1.66
34125	3.49	3.05	3.01	4.05	1.63
43215	2.99	3.89	2.21	5.05	1.48
Average results					
–	3.56	**4.19**	2.52	**3.92**	1.562

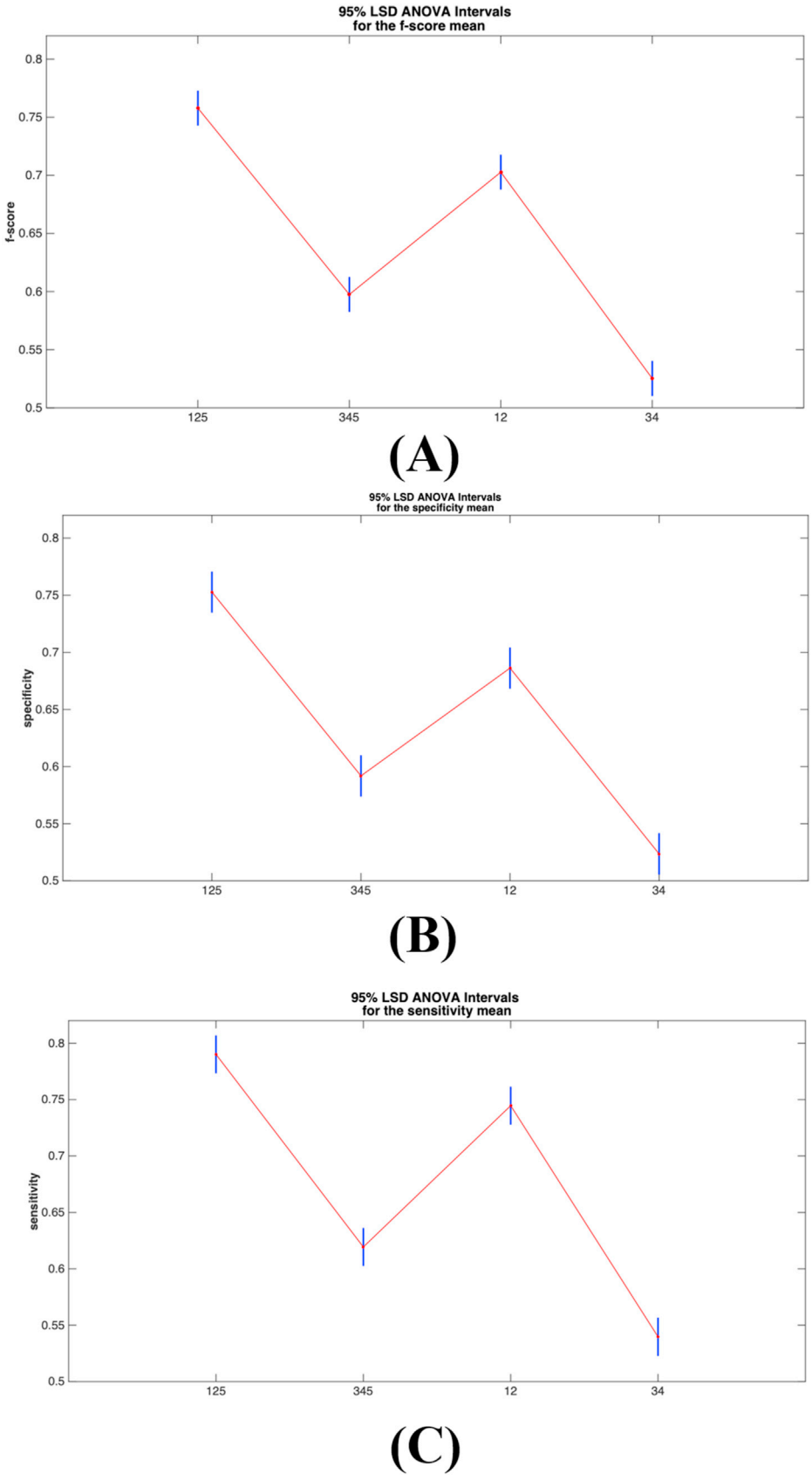

Fig. 5. 95% ANOVA LSD intervals for the average f-score (A), specificity (B), and sensitivity (C), of the different block configurations after removing some of them. The code for the configurations is defined in Table 1.

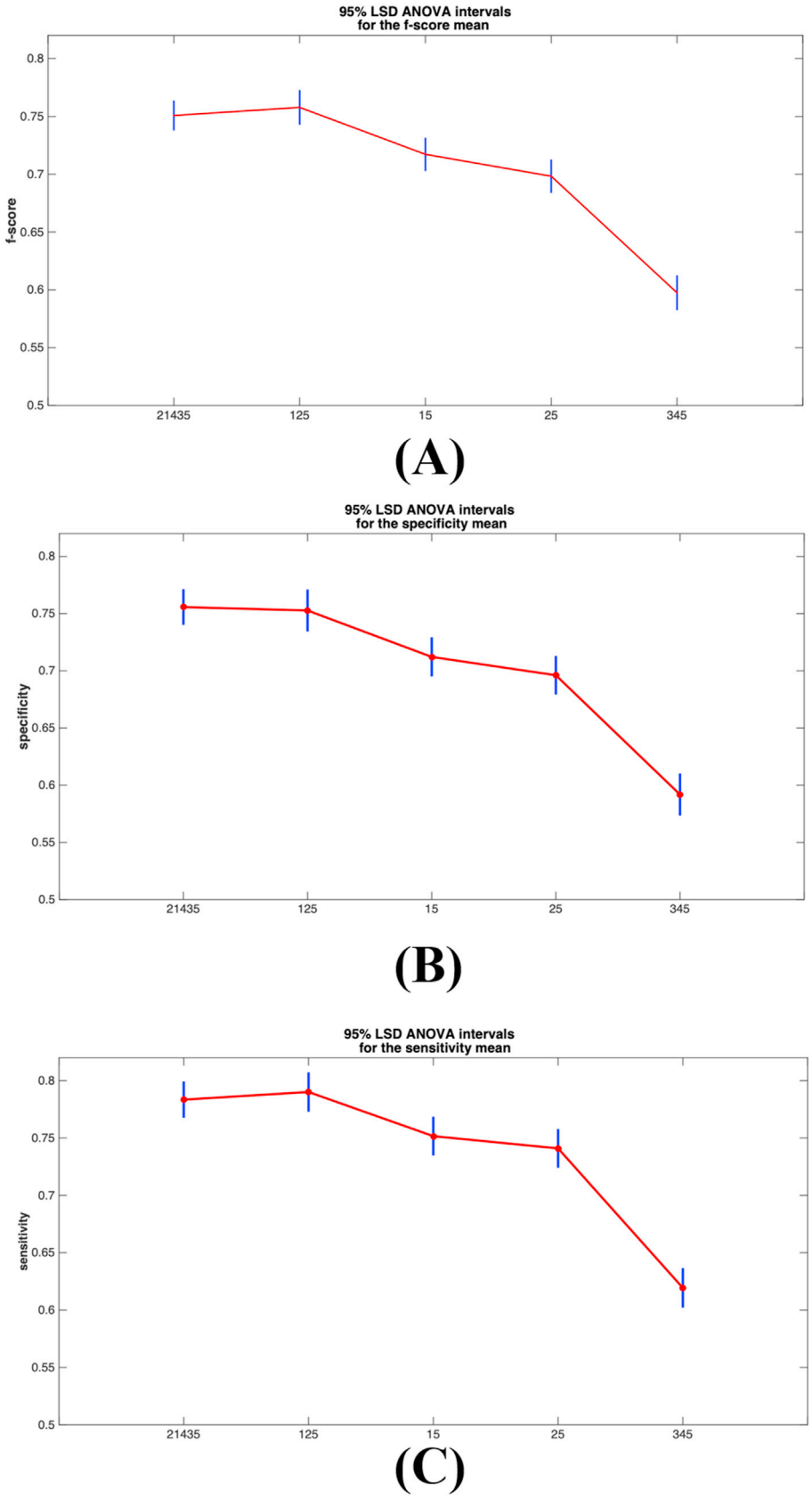

Fig. 6. Summary plot of 95% ANOVA LSD intervals for the average f-score (A), specificity (B), and sensitivity (C). The code for the configurations is defined in Table 1.

Finally, based on the results obtained, configurations 15 and 25 were studied in order to determine if the diffusion blocks (MCR and Exp. Model-based DWI) supply the same information, in that case only one of them is necessary, or contrarily to that, they perform better together.

The statistical significance of the differences between configurations was studied by applying ANOVA with 2 factors: the actual block input configuration and the validation set selection for each iteration (500 runs); the latter used as a blocking factor for decreasing the residual variability and increasing the statistical power. 95% confidence ANOVA least significative differences (LSD) intervals of f-score, sensitivity and specificity (Fig. 4) were obtained for studying the statistical significance of the differences among the different configurations defined in step 1.

As can be observed in Fig. 4, when trying to prioritize pharmacokinetic perfusion models over the other blocks (the configuration 34125), the values obtained were statistically worse (p-value < 0.05) than in the other configurations for all the performance indexes (f-score, sensitivity and specificity), loosing prediction performance. There are no statistically significant differences between the performance indexes for the other configurations. This result can be interpreted as the pharmacokinetic models (block 3) are not a good reference (starting point) in the algorithm for discriminating tumor aggressiveness.

In the next Table, the block importance is studied by showing the number of optimal LV selected for each block in terms of averages:

Table 2 illustrates that the number of LV tend to decrease when the block is sequenced later, because there is less orthogonal information left. It should be highlighted that both MCR blocks (2 and 4) were constantly represented with high number of LV, independently of the position they were sequenced as they obtained the best global average results (Table 2). However, if block 3 is introduced first, the algorithm, generally, will extract a higher number of orthogonal LV than it would normally do from a block that does not provide discriminant power. This causes the elimination of part of the correlated information (because there will be always correlation between blocks) from the others blocks with block 3 that could really provide relevant information, resulting in loss of prediction performance (as seen in Fig. 4).

Once the importance of the block order has been analyzed, the second step for analyzing the block importance was performed as described before. The results provided by a new 2-factor ANOVA that was calculated for checking statistically significant differences between the first four proposed configurations (125, 345, 12 and 34) are shown in Fig. 5.

As shown in Fig. 5, there are statistically significant differences (p-value <0.05) between the proposed sequences. First of all, diffusion blocks (1 and 2) should not be taken out of the model because all the performance indexes (f-score, sensitivity and specificity) of sequences 345 and 34 were statistically worse than those of sequences 125 and 12. Besides, the T2w block appeared to be relevant and it statistically improved the model when it was included (125 was statistically better than 12; and 345 was statistically better than 34).

Finally, one last analysis was proposed in order to compare the performance of the model containing all the blocks in one of the best configurations (21435) with the best model when removing perfusion (125) or diffusion (345). Additionally, the configurations 15 and 25 were also compared with 125 in order to check the importance of the diffusion models individually (MCR-ALS versus Exp. Model-based DWI). The results obtained are shown in Fig. 6.

These results highlight different relevant ideas:

- First, they indicate that perfusion blocks (3 and 4) can be removed from the study, since they provided the worst results, and there were no statistically significant differences between the best models considering all the blocks (e.g. 21435) and the models where only diffusion sequences and T2w images were used (125). This conclusion is relevant because perfusion is an invasive (more harmful for the patients than diffusion) and costly method that needs better equipment and higher functional resolution. Moreover, the computation time is higher for perfusion pharmacokinetic models than for clinical diffusion exponential and MCR-based models (5 and 1 min/pixel, respectively). Besides, when comparing the best configuration (125) with the worst one (34), the differences in performance indices were statistically significant (p-values<0.05) resulting in an estimated average difference of 0.23 points for the f-score, 0.26 for the sensitivity and 0.23 for the specificity. These values represent a relevant increment of more than 25% in prediction performance when using diffusion and T2w instead of only perfusion blocks.
- Second, when trying to use only one of the diffusion blocks (15 and 25), all the performance indexes (f-score, sensitivity and specificity) experienced a statistically significant decrease with respect to the combination of both diffusion blocks (125), losing 0.05 points on average in the performance indices. This result determines that blocks 1 and 2 are complementary and perform better together.

With regards to the limitations of the method, our database was relatively small (36 patients). For further validation, it should be increased with new characterized cases. Future studies including larger cohorts are necessary in order to assess the clinical significance and impact of the results obtained in this paper. Besides, this analysis was performed at the tumor region level, which means that the level of detail and characterization is lower than the pixel level approximation, but the classification and the predictive power increases (is easier to classify regions than pixels). The detection of smaller areas (i.e. a few pixels inside a larger ROI) showing pathological behavior becomes difficult. This limitation is intrinsic to our method, as our gold reference was biopsy, obtained from a certain area, so it is not possible to establish an exact spatial correspondence between biopsy and pixels. One way to partially overcome this is by using radical prostatectomy specimens as gold standard, where the anatomy of the prostate is more preserved and it is more feasible to establish an accurate spatial correspondence. Unfortunately, these samples were not available in this study.

4. Conclusions

SMB-PLS has shown its potential for selecting the best blocks of information related to the different magnetic resonance techniques. Diffusion blocks (1 and 2) have arisen as the best sources of information joint to T2w block (5), providing f-score, sensitivity and specificity values of 0.76, 0.79 and of 0.75, respectively. On the other hand, perfusion blocks (3 and 4) did not provide any additional relevant information. Their capability for grading prostate tumor aggressiveness is statistically lower than using diffusion and T2w images, and thus can be neglected reducing the time the patient is undergoing radiological tests and speeding the delivery of radiologic reports. In addition, T2w does not imply any additional cost as it is mandatory for PI-RADS in the clinical routine. These results are statistically better than using only clinical models separately as done in other studies [36].

ANNEX 1: PSEUDO-CODE OF THE SMB-ALGORITHM

For *b*= 1,2 … *B*-1

1. Set $\mathbf{u}$ to any column of $\mathbf{Y}$ as an initialization
2. Begin the convergence loop

2.1. $\mathbf{w}_b = \mathbf{X}_b^T \cdot \mathbf{u}/(\mathbf{u}^T \cdot \mathbf{u})$

2.2. $\mathbf{w}_b = \mathbf{w}_b/\|\mathbf{w}_b\|$

2.3. $\mathbf{t}_b = \mathbf{X}_b \cdot \mathbf{w}_b$

For *k* = 1,2 … *B*-*b*

2.4. $\mathbf{X}_{b+k}^{corr} = \mathbf{t}_b \cdot \left(\mathbf{t}_b^T \cdot \mathbf{t}_b\right)^{-1} \cdot \mathbf{t}_b^T \cdot \mathbf{X}_{b+k}$

2.5. $\mathbf{w}_{b+k}^{corr} = \mathbf{X}_{b+k}^{Tcorr} \cdot \mathbf{u}/(\mathbf{u}^T \cdot \mathbf{u})$

2.6. $\mathbf{w}_{b+k}^{corr} = \mathbf{w}_{b+k}^{corr}/\|\mathbf{w}_{b+k}^{corr}\|$

2.7. $\mathbf{t}_{b+k}^{corr} = \mathbf{X}_{b+k}^{corr} \cdot \mathbf{w}_{b+k}^{corr}$

End

2.8. $\mathbf{T} = [\mathbf{t}_b\ \mathbf{t}_{b+1}^{corr} \ldots\ \mathbf{t}_B^{corr}]$

2.9. $\mathbf{w}_T = \mathbf{T}^T \cdot \mathbf{u}/(\mathbf{u}^T \cdot \mathbf{u})$

2.10. $\mathbf{w}_T = \mathbf{w}_T/\|\mathbf{w}_T\|$

2.11. $\mathbf{t}_T = \mathbf{T}^T \cdot \mathbf{w}_T/\left(\mathbf{w}_T^T \cdot \mathbf{w}_T\right)$

2.12. $\mathbf{q} = \mathbf{Y}^{\mathrm{T}} \cdot \mathbf{t}_{\mathrm{T}} / \left(\mathbf{t}_{\mathrm{T}}^{\mathrm{T}} \cdot \mathbf{t}_{\mathrm{T}}\right)$

2.13. $\mathbf{u} = \mathbf{Y} \cdot \mathbf{q} / (\mathbf{q}^{\mathrm{T}} \cdot \mathbf{q})$

Loop until convergence on $\mathbf{t}_{\mathrm{T}}$ or $\mathbf{u}$. Go to step 3 when converged.

3. **For** $k = b, b+1 \ldots B$

3.1. $\mathbf{p}_{\mathrm{k}} = \mathbf{X}_{\mathrm{k}}^{\mathrm{T}} \cdot \mathbf{t}_{\mathrm{T}} / \left(\mathbf{t}_{\mathrm{T}}^{\mathrm{T}} \cdot \mathbf{t}_{\mathrm{T}}\right)$

3.2. $\mathbf{E}_{\mathrm{k}} = \mathbf{X}_{\mathrm{k}} - \mathbf{t}_{\mathrm{T}} \cdot \mathbf{p}_{\mathrm{k}}^{\mathrm{T}}$

End

4. $\mathbf{F} = \mathbf{Y} - \mathbf{t}_{\mathrm{T}} \cdot \mathbf{q}^{\mathrm{T}}$
5. Store all vectors at the block and super levels as new columns in matrices.
6. To compute the next LV, replace $\mathbf{X}_{\mathrm{k}}$ by $\mathbf{E}_{\mathrm{k}}$ ($k \geq b$) and $\mathbf{Y}$ by $\mathbf{F}$ and go back to step 1.
7. When the relevant info in block $\mathbf{X}_{\mathrm{b}}$is depleted, increment b and start at step 1. Using $\mathbf{X}_{\mathrm{b}}$ and $\mathbf{Y}$ residuals.

End

8. For $b = B$, fit a regular PLS model to $\mathbf{E}_{\mathrm{B}}$ and $\mathbf{F}$.

(*continued*).

CRediT AUTHOR STATEMENT

Eric Aguado-Sarrió: Conceptualization, Methodology, Software, Validation, Formal analysis, Writing- Original Draft, Writing – Review & Editing, Visualization. José Manuel Prats-Montalbán: Conceptualization, Validation, Writing – Review & Editing, Visualization, Funding acquisition. Roberto Sanz-Requena: Conceptualization, Validation, Resources, Data curation, Writing – Review & Editing. Carl Duchesne: Software, Validation, Writing – Review & Editing. Alberto Ferrer: Conceptualization, Validation, Writing – Review & Editing, Supervision.

Declaration of competing interest

The authors declare that they have no known competing financial interests or personal relationships that could have appeared to influence the work reported in this paper.

Acknowledgements

This research was partially supported by the Spanish Government (Science and Innovation Ministry) under the project PID2020-119262RB-I00, and by the Generalitat Valenciana under the project AICO/2021/111.

References

[1] R. Alonzi, P. Hoskin, Functional imaging in clinical oncology: magnetic resonance imaging – and computerised tomography-based techniques, Clin. Oncol. 18 (7) (2006) 555–570.
[2] D.J. Collins, A.R. Padhani, Dynamic magnetic resonance imaging of tumor perfusion, IEEE Eng. Med. Biol. Mag. 23 (2004) 65–83.
[3] G. Giannarini, G. Petralia, H.C. Thoeny, Potential and limitations of diffusion-weighted magnetic resonance imaging in kidney, prostate and bladder cancer including pelvic lymph node staging: a critical analysis of the literature, Eur. Urol. 61 (2012) 326–340.
[4] S.W. Heijmink, J.J. Fütterer, S.S. Strum, W.J. Oyen, F. Frauscher, J.A. Witjes, et al., State-of-the-art uroradiologic imaging in the diagnosis of prostate cancer, Acta Oncol. 50 (Suppl. 1) (2011) 25–38.
[5] D. Le Bihan, Molecular diffusion nuclear magnetic resonance imaging, Magn. Reson. Q. 7 (1991) 1–30.
[6] American College of Radiology, MR Prostate Imaging Reporting and Data System Version 2.0. http://www.acr.org/Quality-Safety/Resources/PIRADS/. (Accessed February 2022).
[7] A.J. Atkinson, W.A. Colburn, V.G. Degruttola, D.L. Demets, Biomarkers and surrogate end-points: preferred definitions and conceptual framework, Clin. Pharmacol. Ther. 69 (2001) 89–95.
[8] P.S. Tofts, G. Brix, D.L. Buckley, J.L. Evelhoch, E. Henderson, M.V. Knopp, et al., Estimating kinetic parameters from dynamic contrast-enhanced T1-weighted MRI of a diffusable tracer: standardized quantities and symbols, J. Magn. Reson. Imag. 10 (1999) 223–232.
[9] A. Szafer, J. Zhong, A.W. Anderson, J.C. Gore, Diffusion-weighted imaging in tissues: theoretical models, NMR Biomed. 8 (7–8) (1995) 289–296.

[10] D. Le Bihan, E. Breton, D. Lallemand, P. Grenier, E. Cabanis, M. Laval-Jeantet, MR imaging of intravoxel incoherent motions: application to diffusion and perfusion in neurologic disorders, Radiology 161 (1986) 401–407.
[11] A. De Juan, R. Tauler, Multivariate curve resolution (MCR) from 2000: progress in concepts and applications, Crit. Rev. Anal. Chem. 36 (3–4) (2006) 163–176.
[12] R. Tauler, A.K. Smilde, B.R. Kowalski, Selectivity local rank, three-way data analysis and ambiguity in multivariate curve resolution, J. Chemom. 9 (1995) 31–58.
[13] Multivariate Curve Resolution Homepage. http://www.mcrals.info/. (Accessed February 2022).
[14] J.M. Prats-Montalbán, R. Sanz-Requena, L. Martí-Bonmatí, A. Ferrer, Prostate functional magnetic resonance image analysis using multivariate curve resolution methods, J. Chemom. 28 (8) (2014) 672–680.
[15] E. Aguado-Sarrió, J.M. Prats-Montalbán, R. Sanz-Requena, A. Alberich-Bayarri, L. Martí-Bonmatí, A. Ferrer, Prostate diffusion weighted-magnetic resonance image analysis using multivariate curve resolution methods, Chemometr. Intell. Lab. Syst. 140 (2015) 43–48.
[16] J.M. Prats-Montalbán, E. Aguado-Sarrió, A. Ferrer, Multivariate Curve Resolution for Magnetic Resonance Image analysis: applications in prostate cancer biomarkers development, in: Resolving Spectral Mixtures, with Application from Ultrafast Spectroscopy to Super-resolution Imaging, Data Handling in Science and Technology vol. 30, Elsevier, Amsterdam, 2016, pp. 519–550.
[17] E. Aguado-Sarrió, Application of Multivariate Image Analysis to Prostate Cancer for Improving the Comprehension of the Related Physiological Phenomena and the Development and Validation of New Imaging Biomarkers, PhD Thesis, Universitat Politècnica de València, Valencia, Spain, 2019.
[18] P. Geladi, B.R. Kowalski, Partial least-squares regression: a tutorial, Anal. Chim. Acta 185 (1986) 1–17.
[19] M. Sjöström, S. Wold, B. Söderström, PLS Discriminant Plots, Proceedings of PARC in Practice, Amsterdam, Elsevier Science Publishers B.V., North-Holland, 1986. June 19-21, 1985.
[20] Lauzon-Gauthier J, Duschesne C. A new multiblock PLS algorithm including a sequential pathway. In: EuroPact 2014, May 6-9, 2014, Barcelona, Spain. 130.
[21] K. Azari, J. Lauzon-Gauthier, C. Tessier, C. Duchesne, Establishing multivariate specification regions for raw materials using SMB-PLS, in: Proceedings of the 9th IFAC Symposium on Advanced Control of Chemical Processes", ADCHEM 2015, 2015, pp. 1132–1137. Whistler, BC, Canada.
[22] J. Lauzon-Gauthier, P. Manolescu, C. Duchesne, The sequential multi-block PLS algorithm (SMB-PLS): comparison of performance and interpretability, Chemometr. Intell. Lab. Syst. 180 (2018) 72–83.
[23] G.P. Murphy, C. Busch, P.A. Abrahamson, J.I. Epstein, J.E. McNeal, G.J. Miller, et al., Histopathology of localized prostate cancer. In *consensus Conference on Diagnosis and prognostic Parameters in localized prostate cancer*. Stockholm, Sweden, may 12-13, 1993, Scand. J. Urol. Nephrol. Suppl. 162 (1994) 7, discussion 115-27.
[24] E. Aguado-Sarrió, J.M. Prats-Montalbán, R. Sanz-Requena, G. Garcia-Martí, L. Martí-Bonmatí, A. Ferrer, Biomarker comparison and selection for prostate cancer detection in dynamic contrast enhanced-magnetic resonance imaging (DCE-MRI), Chemometr. Intell. Lab. Syst. 165 (2017) 38–45.
[25] J.E. Jackson, A User's Guide to Principal Components, Wiley, New York, 2003.
[26] R. Sanz-Requena, J.M. Prats-Montalbán, L. Martí-Bonmatí, A. Alberich-Bayarri, G. García-Martí, R. Pérez, A. Ferrer, Automatic individual arterial input functions calculated from PCA outperform manual and population-averaged approaches for the pharmacokinetic modeling of DCE-MR images, J. Magn. Reson. Imag. 42 (2015) 477–487.
[27] D. Le Bihan, E. Breton, D. Lallemand, M.L. Aubin, J. Vignaud, M. Laval-Jeantet, Separation of diffusion and perfusion in intravoxel incoherent motion MR imaging, Radiology 168 (2) (1988) 497–505.
[28] S.P. Sourbron, D.L. Buckley, Tracer Kinetic modelling in MRI: estimating perfusion and capillary permeability, Phys. Med. Biol. 57 (2) (2012) R1–R33.
[29] M.O. Leach, K.M. Brindle, J.L. Evelhoch, J.R. Griffiths, M.R. Horsman, A. Jackson, et al., Assessment of antiangiogenic and antivascular therapeutics using MRI: recommendations for appropriate methodology for clinical trials, Br. J. Radiol. 76 (Spec Nº 1) (2003) S87–S91.
[30] L. Lüdemann, D. Prochnow, T. Rohlfing, T. Franiel, C. Warmuth, M. Taupitz, et al., Simultaneous quantification of perfusion and permeability in the prostate using dynamic contrast-enhanced magnetic resonance imaging with an inversion-prepared dual sequence, Ann. Biomed. Eng. 2 (37) (2009) 749–762.
[31] P. Geladi, Grahn, Multivariate Image Analysis, Wiley, Chichester, England, 1996.
[32] J.M. Prats-Montalbán, A. Ferrer, A. de Juan, Multivariate image analysis: a review with applications, Chemometr. Intell. Lab. Syst. 107 (2011) 1–23.
[33] M.J. Bruwer, J.F. MacGregor, D. Noseworthy, Dynamic contrast-enhanced MRI diagnosis in oncology via principal component analysis, J. Chemom. 22 (2008) 708–716.
[34] A. De Juan, M. Maeder, T. Hancewicz, L. Duponchel, R. Tauler, Chemometric tools for image analysis, in: Infrared and Raman Spectroscopic Imaging, Wiley-VCH Verlag Gmbh & Co. KGaA, 2009, pp. 65–109.
[35] J. Jaumot, R. Tauler, MCR-BANDS: a user friendly MATLAB program for the evaluation of rotation ambiguities in multivariate curve resolution, Chemometr. Intell. Lab. Syst. 103 (2010) 96–107.
[36] R. Sanz-Requena, L. Martí-Bonmatí, R. Pérez-Martínez, G. García-Martí, Dynamic contrast-enhanced case-control analysis in 3T MRI of prostate cancer can help to characterize tumor aggressiveness, Eur. J. Radiol. 85 (2016) 2119–2126.